Front. Environ. Sci. Eng. 2024, 18(2): 14
https://doi.org/10.1007/s11783-024-1774-9

RESEARCH ARTICLE

Partial aging can counter-intuitively couple with sulfidation to improve the reactive durability of zerovalent iron

Yiwei Liu[1], Kaili Gu[1], Jinhua Zhang[1], Jinxiang Li (✉)[1], Jieshu Qian[1], Jinyou Shen[1], Xiaohong Guan (✉)[2]

1 Jiangsu Key Laboratory of Chemical Pollution Control and Resources Reuse, School of Environmental and Biological Engineering, Nanjing University of Science and Technology, Nanjing 210094, China
2 School of Ecological and Environmental Sciences, East China Normal University, Shanghai 200241, China

HIGHLIGHTS

- Partial aging of SZVI can enhance its reactive durability toward Cr(VI).
- Partial aging can couple with sulfidation to reconstruct the interface of ZVI.
- Partial aging can retain the conductive FeS_x in the subshell of SZVI.
- Iron (hydr)oxides and FeS_x improve the mass and electron transfer of ZVI to Cr(VI).

ARTICLE INFO

Article history:
Received 19 May 2023
Revised 25 June 2023
Accepted 18 July 2023
Available online 5 September 2023

Keywords:
Zerovalent iron
Sulfidation
Partial aging
Interface reconstruction
Electron transfer

GRAPHIC ABSTRACT

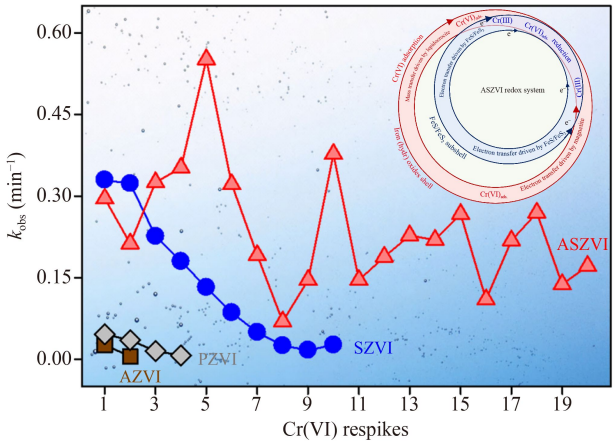

ABSTRACT

Sulfated zero-valent iron (SZVI) has shown promising applications in wastewater treatment. However, the rapid decline in the reactivity of SZVI with time limits its real practice. To mediate this problem, partial aging was proposed to improve the reactive durability of SZVI. Taking Cr(VI) as the target contaminant, we found that the aged ZVI (AZVI) gradually lost reactivity as aging time increased from 0.5 to 2 d. Counter-intuitively, the partially aged SZVI (ASZVI) showed greater reactivity than SZVI when exposed to oxygenated water for a period ranging from 0.5 to 14 d. In addition, the ASZVI with 0.5 d of aging time (ASZVI-0.5) not only maintained reactivity in successive runs but also increased the Cr(VI) removal capacity from 9.1 mg/g by SZVI to 19.1 mg/g by ASZVI-0.5. Correlation analysis further revealed that the electron transfer from the Fe^0 core to the shell was mediated by the conductive FeS and FeS_2 in the subshell of ASZVI. Meanwhile, the lepidocrocite and magnetite on the surface of ASZVI facilitated Cr(VI) adsorption and subsequent electron transfer for Cr(VI) reduction. Moreover, the iron (hydr)oxide shell could retain the conductive FeS and FeS_2 in the subshell, allowing ASZVI to reduce Cr(VI) efficiently and sustainably. In general, partial aging can enhance the reactive durability of ZVI when coupled with sulfidation and this synergistic effect will be beneficial to the application of SZVI-based technology for wastewater treatment.

1 Introduction

Over the past decades, zerovalent iron (ZVI) has been proven to be an environmentally friendly and commercially available material for groundwater remediation and wastewater treatment (Gillham and Ohannesin, 1994; Matheson and Tratnyek, 1994; Fu et al., 2014; Guan et al., 2015; Liu et al., 2022). Various organic and inorganic contaminants can be removed from water

✉ Corresponding authors
E-mails: lijx@njust.edu.cn (J. Li); xhguan@des.ecnu.edu.cn (X. Guan)

by ZVI through oxidation, reduction, adsorption, and/or co-precipitation (Miehr et al., 2004; Noubactep, 2008; Yoon et al., 2011; Fu et al., 2014; Liang et al., 2014b; Guan et al., 2015; Li et al., 2015; 2020b). In these processes of contaminants removal, ZVI corrodes and then is converted to a variety of iron (hydr)oxides (Liang et al., 2014b; Liu et al., 2022). Although these iron (hydr)oxides can increase the surface area of ZVI for contaminants adsorption, most of them (e.g., α-Fe_2O_3, γ-Fe_2O_3, α-FeOOH, γ-FeOOH, δ-FeOOH) are non-conductive and thus unbeneficial for the contaminants reduction by ZVI (Liang et al., 2014a; 2014b; Shao et al., 2018; Sun et al., 2014). In addition, as the decontamination proceeds, these iron (hydr)oxides accumulate on the surface of ZVI to form a dense passive film, which further impedes the mass transfer and electron transfer between the contaminant and ZVI (Guan et al., 2015; Fan et al., 2021; Liu et al., 2022). Therefore, the reactivity of ZVI declines rapidly over time, especially when ZVI is deployed for water treatment under aerobic conditions.

To mediate this problem, many methods have been developed to disrupt or modulate the distribution of iron (hydr)oxides on the surface of ZVI (Guan et al., 2015), including acid washing (Agrawal and Tratnyek, 1995), H_2 pretreatment (Liou et al., 2005), ultrasonication (Geiger et al., 2002), dosing chemicals (e.g., Fe^{2+} or oxidants) (Qin et al., 2017, Fan et al., 2019a; Ullah et al., 2020), and externalization of weak magnetic field (WMF) (Liang et al., 2014a), etc. Although these strategies can enhance the initial reactivity of ZVI toward the target contaminant, they are also able to accelerate the side-reaction of ZVI with the natural substances (e.g., O_2, and H_2O/H^+), which results in the waste of Fe^0 content and thus reducing the reductive durability of ZVI against the target contaminants. In the past decade, the application of sulfidation to improve the reactivity and electron efficiency of ZVI for contaminant reduction has gained significant interest (Fan et al., 2017; Li et al., 2017; Fan et al., 2019a; Garcia et al., 2021; Zhao et al., 2021). To date, studies have found that the sulfidation of ZVI (SZVI) can be achieved by aqueous-solid reactions (Xu et al., 2016a; Huang et al. 2018; Li et al. 2018; Shao et al., 2018; Li et al., 2020a) or solid-solid reactions (Gu et al., 2017; Li et al., 2018; Gu et al., 2019; Zou et al., 2019; Cai et al., 2021). By replacing the unwanted passive films, the newly formed (i.e., FeS_x) can provide the inner host (Fe^0) with better electrical conductivity and larger surface area/roughness (Kim et al., 2011; Fan et al., 2017; Li et al., 2017; Li et al., 2018; Ling et al., 2019; Lü et al., 2019; Qiao et al., 2021; Huang et al., 2022). As a result, the reactivity of ZVI with sulfidation was generally higher than that without sulfidation (Fan et al., 2017; Li et al., 2017; Song et al., 2017, Xu et al., 2020c; Garcia et al., 2021). Moreover, due to the superior hydrophobicity of FeS and FeS_2, sulfidation can inhibit the side reaction of ZVI with oxygen-free water (Rajajayavel and Ghoshal, 2015; Qin et al., 2018; Mangayayam et al., 2019), thereby prolonging the reactive lifetime of ZVI for contaminants reduction under anaerobic conditions.

Recently, there has been a growing interest in using SZVI for the sequestration of various contaminants in aerobic water (Xu et al., 2016a; Huang et al., 2018; Li et al. 2018; Fan et al. 2019b; Ling et al., 2019; Li et al., 2020a). Disappointingly, Xu et al. (2016a) verified that there was a gradual decrease in the reaction rates for decolorization of Orange I by SZVI in consecutive tests under aerobic conditions. We also found that the reactivity of SZVI decreased progressively when Cr(VI) was successively removed in an open (aerobic) stirred batch reactor (Li et al., 2018). Moreover, the decline in the reactivity of SZVI was generally accompanied by a drop in the total content of S_2^{2-} and S^{2-} in the SZVI sample (Li et al., 2018). Therefore, it can be inferred that the oxidation of FeS and FeS_2 in SZVI particles by the strong oxidizing species (e.g., Cr(VI)) should be the possible cause of the declined reactivity of SZVI with time. In other words, sustaining the contents of iron sulfides (FeS_x) in SZVI should be an effective route to maintain its reactive durability.

In essence, reconstructing the interface of SZVI to obtain a stable reactive interface should be the key way to maintain the excellent reactivity of SZVI. It has been clarified that aging generally makes the surface of ZVI consist of magnetite and lepidocrocite (Liang et al., 2014b; Xu et al. 2016b; Zhang et al. 2018), which are beneficial for the electron and mass transfer of the ZVI system to remove contaminants (Qin et al., 2017; Shao et al. 2018). In light of such interaction, if SZVI is properly aged for a certain period of time (referred to as 'partial aging' in this study), the interface of SZVI can be reconstructed to form a sandwich structure consisting of Fe^0 core, FeS_x interlayer, and iron (hydr)oxide surface. In this reconstructed structure, the desired shells of magnetite and lepidocrocite not only facilitate the mass transfer and electron transfer for contaminants removal but also may protect the FeS and FeS_2 in the SZVI from being wasted under aerobic conditions. Therefore, partial aging may have a positive effect on the reactive durability of SZVI. However, this view is mainly hypothetical and needs further validation. Furthermore, the structure-activity relationships involved in the reaction between contaminants and reconstructed SZVI are not well understood.

Accordingly, partial aging is proposed in this study to reconstruct the interface of SZVI to improve its reactive durability. Also, hexavalent chromium (Cr(VI)), a suspected carcinogen to organisms and widely present in industrial wastewater (Feng et al., 2015; Gheju 2011), is selected as the target contaminant in this study. The overall objectives of this work are to: 1) reconstruct the interface of SZVI with aging time ranging from 0.5 to

14 d and semi-quantify the spatial distributions of sulfur and iron species in these partially aged SZVI (ASZVI) samples; 2) explore the coupled effects of sulfidation and partial aging on the reactive durability of ZVI under aerobic conditions, and 3) elucidate the contributions of the FeS_x interlayer and iron (hydr)oxide shell to sustainably enhance the removal of Cr(VI) by ZVI.

2 Experimental sections

2.1 Chemicals and materials

All chemicals used in this study were of analytical grade and purchased from Aladdin Reagent Co. Ltd., China. The micro-size pristine ZVI (PZVI) employed in this study is high purity Fe^0 (> 99.0%) with a mean diameter of 103.95 μm and BET surface area of 0.0577 m^2/g. The stock and reaction solutions were prepared with the ultrapure water produced by a Milli-Q water purification system. The details for synthesizing the aged ZVI (AZVI) and SZVI samples were analogous to our previous studies (Liang et al., 2014b; Xu et al., 2016b) and described in Text S1 of the Supporting Information (SI). As for the preparation of ASZVI samples, 10.0 g of SZVI was incubated in 0.5 L of distilled water open to the air, which was buffered with 0.20 mol/L 2-(N-morpholino) ethanesulfonic acid (MES). Then, it was mixed with a mechanical stirrer at 100 r/min for 0.5, 1, 2, 4, 7, or 14 d, and the obtained samples were denoted as ASZVI-0.5, ASZVI-1, ASZVI-2, ASZVI-4, ASZVI-7, and ASZVI-14, respectively. All samples were filtered, washed with DI water, vacuum-dried, and kept in anaerobic sealed bags for subsequent characterization and use.

2.2 Batch experiments

All experiments were conducted open to the air and mixed at 400 r/min with a mechanical stirrer. The temperature of the reaction solution was controlled at 25 °C with a water bath. For a typical batch test, briefly, 0.25 g as-prepared sample was added into 0.5 L working solution containing 4.0 mg/L Cr(VI). Unless stated otherwise, 1.0 mmol/L Na_2SO_4 was employed as the background electrolyte. All bath tests were repeated at least two times, and the error bars in the figures showed the standard deviation.

For the re-spiking experiments with Cr(VI), they were conducted in one batch within 540 min to investigate the consecutive removal performance of Cr(VI) by the PZVI, AZVI, SZVI, and ASZVI-0.5, respectively. The time intervals between two spikes were determined by the period for almost elimination of Cr(VI) from water. To initiate the first spike, a 1.0 g as-prepared sample was dosed into the unbuffered working solution containing 2.0 mg/L Cr(VI) and 1.0 mmol/L NaCl as the background electrolyte. After the exhaustion of Cr(VI), a certain amount of 200 mg/L Cr(VI) stock solution was transferred to maintain the same concentration of Cr(VI) (~2.0 mg/L) at the beginning of every cycle. It should be noted that the initial pH (pH_{ini}) of the reaction solution in all the experiments was adjusted to 5.0 with NaOH and H_2SO_4 and no buffer was used.

2.3 Analysis and characterizations

At the specified time intervals, 2 mL of suspension was immediately collected and filtered through a 0.22 μm filter membrane. After acidification, the concentration of Cr(VI) was measured with the diphenylcarbazide colorimetric method using a UV-Vis spectrophotometer (UV-9600, Beijing Ruili Analytical Instrument Co. Ltd.) at 540 nm (Feng et al., 2015). The concentration of ferrous iron was determined with the 1,10-phenanthroline colorimetric method using an UV-Vis spectrophotometer at 510 nm (Stookey, 1970). The morphology of the as-prepared ZVI samples was characterized by scanning electron microscopy (SEM, ZEISS Gemini 300) fixed with EDX elemental mapping. The specific surface areas of the ZVI-based samples were determined by the BET method (Micrometrics ASAP 3020). Raman spectra of the ZVI-based samples were collected by a Raman spectrometer (LabRAM ARAMIS) with a 532 nm argon ion laser and a CCD matrix detector. The spatial iron and sulfur species of the ASZVI samples before and after the reaction with Cr(VI) were recorded by X-ray photoelectron spectroscopy (XPS) (ESCALAB 250Xi). Electrochemical tests were carried out by the CHI604E electrochemical workstation (Shanghai Chenhua Instrument Co. Ltd.) to investigate the corrosion properties of the ASZVI samples. More details of the XPS analysis and electrochemical characterization were documented in Text S2 and Text S3 of SI, respectively.

3 Results and discussion

3.1 Effect of partial aging on the interfacial characteristics of ZVI-based materials

As shown in Fig. S1, it was found that both PZVI and SZVI had a smooth and compact surface and they were covered with traces of iron (hydr)oxides. In contrast, the AZVI was severely corroded and its Raman spectrum showed that the major components of the aging film were magnetite, lepidocrocite, maghemite, and goethite. After the partial aging, some spherical particles formed on the surface of the ASZVI samples (Fig. S2). As shown in Fig. 1(a), the Raman spectra of all the synthesized ASZVI samples had a strong peak appearing at around 670 cm^{-1}, which should be the characteristic peak of magnetite (Liang et al., 2014b; Li et al., 2019). In addition, when the

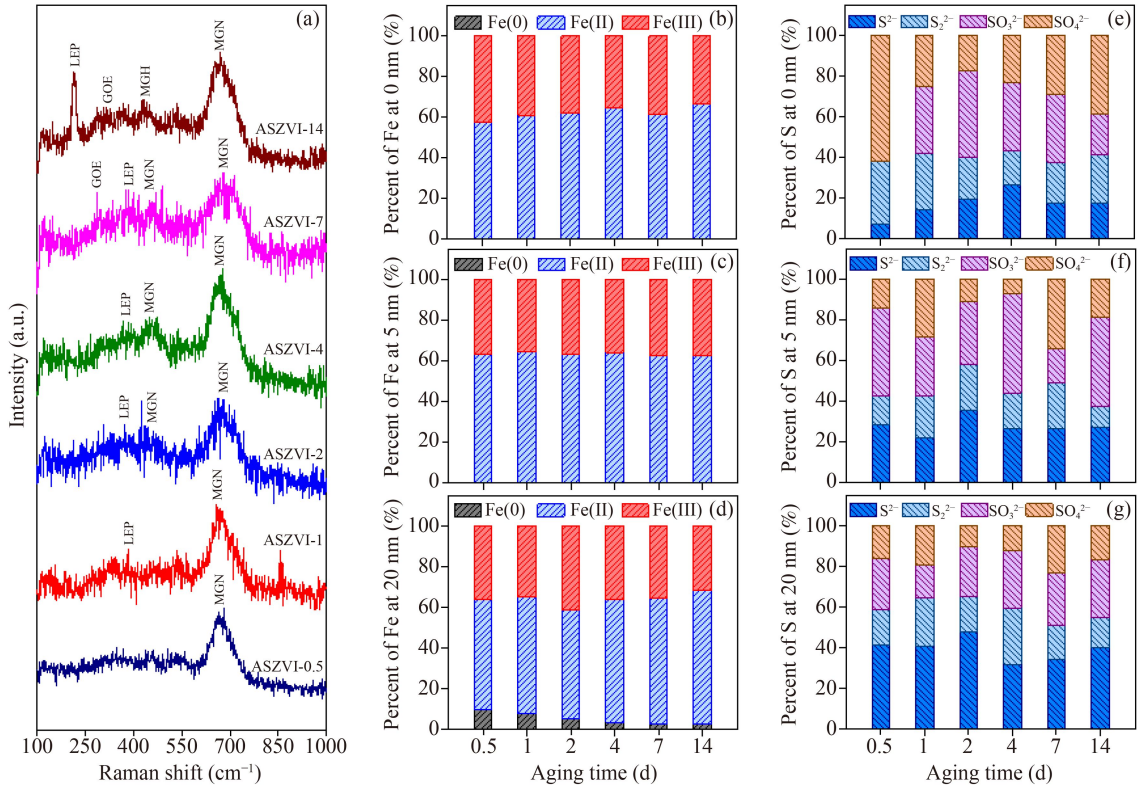

Fig. 1 Effect of aging time on the Raman spectra of the ASZVI samples (a) and the relative contents of Fe species (b–d) and S species (e–g) in the subshell of ASZVI samples from 0 to 20 nm.

aging time was increased from 2 to 14 d, the peaks of lepidocrocite at 245 and 380 cm^{-1} appeared in the Raman spectra of ASZVI samples (Li et al., 2019). Moreover, as shown in Table S1 of the SI, the BET-specific surface areas of ASZVI samples were in the range of 0.2941–1.6657 m^2/g, which were larger than that of PZVI (0.0577 m^2/g) and SZVI (0.0849 m^2/g). The variation in the BET-specific surface areas of ASZVI samples was inconsistent with the monotonically increased surface area of AZVI as a function of the aging time (Liang et al., 2014b), which may be related to the presence of iron sulfides in the interface of ASZVI samples.

To further identify the interfacial element distributions of the ASZVI samples, as shown in Figures S3 and S4, the XPS combined with ion sputtering for depth profiling was used to characterize the ASZVI samples. There were several obvious trends in the collected Fe and S 2p XPS depth profiling spectra of the ASZVI samples: 1) four species of sulfur (i.e., S^{2-}, S_2^{2-}, SO_3^{2-}, and SO_4^{2-}) and two states of iron (i.e., Fe^{2+} and Fe^{3+}) were formed in the interface of the ASZVI samples (Figs. 1(b)–1(g)); 2) The Fe^0 existed only in the subshell of ASZVI samples at 20 nm and its relative content gradually decreased with prolonging the aging period (Fig. 1(d)); 3) Since the main corrosion products at the surface of ASZVI samples were Fe_3O_4 and other Fe(III) (hydr)oxides according to the Raman spectra, the theoretical ratio of Fe(III) to Fe(II) in the interface of ASZVI samples should be greater than or equal to 2. However, the relative contents of Fe(II) were much higher than that of Fe(III) in the subshells of ASZVI samples (Figs. 1(b)–1(d) and Table S2). This deviation largely implied that some Fe(II)-S compounds (e.g., FeS and/or FeS_2) were generated in the interface of the ASZVI samples; 4) The relative content of S^{2-} or the total relative content of S^{2-} and S_2^{2-} in the subshell of ASZVI samples increased with enlarging ion sputtering depth from 0 to 20 nm (Figs. 1(e)–1(g) and Table S3); 5) The total mass content of S^{2-} and S_2^{2-} in the subshell of ASZVI samples remained almost constant with increasing aging time (Table S3), which largely suggested that the iron (hydr)oxides on the shell of ASZVI might prevent the inner FeS_2 and FeS from oxidation by the natural substances (e.g., O_2, and H_2O/H^+).

3.2 Coupled effects of partial aging and sulfidation on the reactive durability of ZVI

As shown in Figure S5(a), sulfidation could significantly improve the efficiency of Cr(VI) removal by PZVI from 23.3% to 42.3%, whereas only about 2.7%–15.0% of Cr(VI) was removed by ZVI aged for 0.5–2.0 d. The negative effect of aging on the reactivity of ZVI had been reported in previous studies (Liang et al., 2014b; Xu et al., 2016b; Zhang et al. 2018), which should be mainly due to the inhibition of the mass transfer and electron transfer between ZVI and Cr(VI). In contrast, the ASZVI

with aging time ranging from 0.5 to 14 d were much more efficient in removing Cr(VI) than SZVI (Fig. S5(b)). To simulate the kinetics of Cr(VI) sequestration by ZVI-based samples, the pseudo-first-order rate law was employed and the obtained rate constants were depicted in Fig. 2(a) and summarized in Table S4. As the partial aging time was increased from 0 to 14 d, the rate constants were gradually increased from 0.0084 min^{-1} for SZVI to 0.0269 min^{-1} for ASZVI-1. Then, they were gradually decreased to 0.0135 min^{-1} for ASZVI-14. The obvious rate constants (k_{obs}) for Cr(VI) removal by ASZVI samples were 1.6–3.2 folds and 5.2–69.3 folds greater than those by SZVI and AZVI samples, respectively.

Figure S6 showed the XPS spectra of the Cr states on the surface of SZVI-based samples after their reaction with Cr(VI). As shown in Fig. 2(b) and Table S5, the Cr(III) content occupied about 83.3% in the Cr-reacted ASZVI-0.5, and then experienced a slight fluctuation with increasing aging time. Therefore, the reduction and adsorption played a joint role in the removal of Cr(VI) by ASZVI samples. The enhanced reactivity of SZVI by partial aging should be attributed to the high conductivity due to their interfacial magnetite, FeS and FeS_2, which facilitates the electron transfer from the Fe^0 core to the shell (Liang et al., 2014b; Xu et al., 2019b; Cao et al., 2020a; Shi et al., 2023). Meanwhile, the iron (hydr)oxides such as lepidocrocite shell could increase the surface area of ASZVI samples for the adsorption of contaminants (Xu et al., 2016b; Huang et al., 2018; Zhang et al., 2018; Yao et al., 2022). However, it should be noted that the contribution of reduction was more significant than that of adsorption in the removal of Cr(VI) by ASZVI samples. The electrical conductivity of ASZVI samples was also investigated by the Tafel polarization curves, as shown in Fig. S7 and listed in Table S6. According to Fig. 2(c), it was found that there was a positive correlation between the lgi_{corr} and the surface normalized rate constants (lgk_{SA}, calculated using Eq. (1)) of the ASZVI samples (Miehr et al., 2004; Li et al., 2015; 2019). This relationship implies that the ASZVI sample is highly dependent on its electron transfer to Cr(VI), as evidenced by the high percentage (over 72.3%) of Cr(III) measured in the Cr-reacted ASZVI samples (Fig. 2(b)).

$$k_{SA} = \frac{k_{obs}}{\rho_a}, \quad (1)$$

where ρ_a is the BET surface area concentration of AZVI samples (m^2/L). Therefore, the unit of k_{SA} is (L·m^2)/min.

The reactive durability of SZVI is especially significant for treating the Cr(VI)-containing wastewater. As such, a consecutive experiment was established to further evaluate the applicability of ASZVI for the consecutive removal of Cr(VI). As shown in Figs. 3(a)–3(c), PZVI and AZVI only achieved 92.2% removal of Cr(VI) at the 4^{th} and 2^{nd} consecutive doses, respectively. In comparison, ASZVI-0.5 demonstrated a remarkable ability to remove nearly 100% of 20 consecutive doses of 2 mg/L Cr(VI) within 540 min. From Fig. 3(d), it could be seen that the rate constants of SZVI for the consecutive removal of Cr(VI) were decreased with the increase of the re-spikes. Although the rate constants for Cr(VI) consecutive removal by ASZVI-0.5 fluctuated with increasing the re-spikes, the reactivity of ASZVI-0.5 was much greater than that of SZVI. Moreover, as demonstrated in Fig. 3(e), the accumulated capacity of Cr(VI) removal by ASZVI-0.5 within 540 min was 19.1 mg/g, which was much higher than that by PZVI (3.7 mg/g), AZVI (1.3 mg/g), and SZVI (9.1 mg/g). Meanwhile, the efficiency of SZVI in reducing Cr(VI) to Cr(III) could be increased from 77.2% to 85.8% in consecutive runs by partial aging. As shown in Figure S8, this study further investigated the effect of water matrix on the reactivity of AZVI-0.5. It was observed that the ASZVI had higher reactivity with Cr(VI) compared to SZVI (Figs. S8(a) and S8b)), with rate constants for ASZVI being 3.4–6.7 times greater than SZVI. In addition, increasing the concentration of 1,10-phenanthroline (Phen) from 0.04 to 0.10 mmol/L could result in a decrease in rate constants for both ASZVI and SZVI (Fig. S8(c)). Specifically, rate constants for Cr(VI)

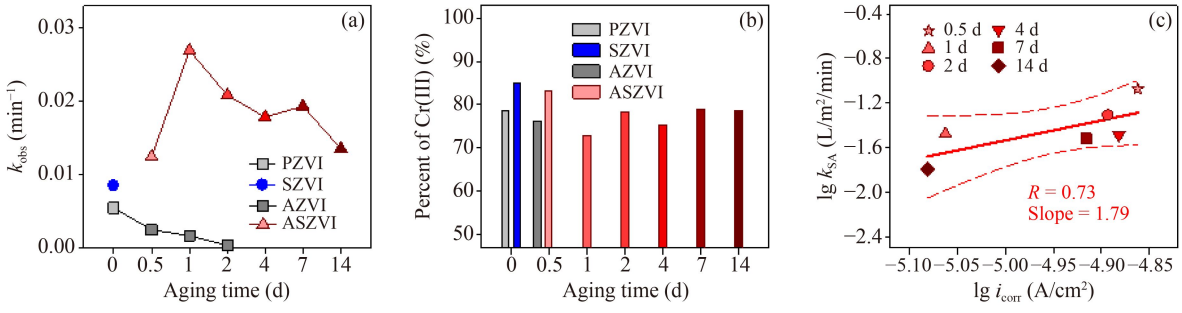

Fig. 2 Influence of aging time on the obvious rate constants (k_{obs}) for Cr(VI) removal by ZVI-based samples (a) and their content of Cr(III) after reaction at 120 min (b). Reaction conditions: $[ZVI]_0$ = 0.5 g/L, $[Cr(VI)]_0$ = 4.0 mg/L, pH_{ini} = 5.0, $[Na_2SO_4]$ = 1.0 mmol/L, t = 25 °C. Relationship of the specific rate constants (lgk_{SA}) for Cr(VI) removal by ASZVI samples with their corrosion current density (c, lgi_{corr}).

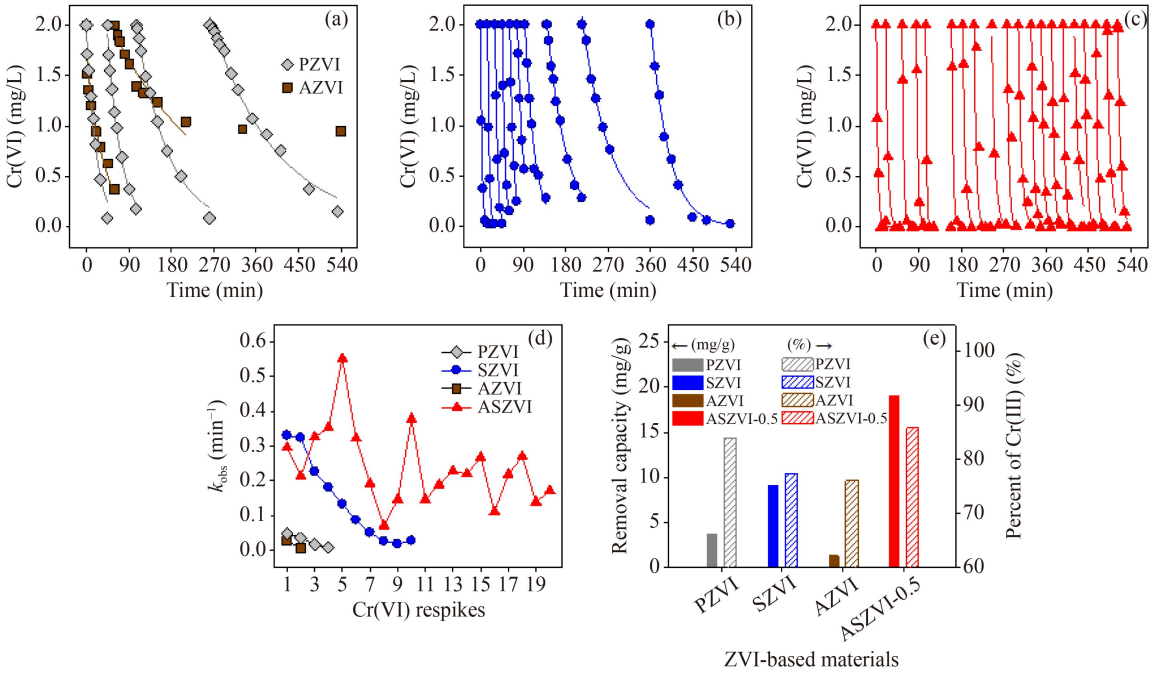

Fig. 3 Kinetics of Cr(VI) removal in consecutive runs by PZVI/AZVI (a), SZVI (b), and ASZVI-0.5 (c), along with their reaction rates (d), removal capacity (e, left ordinate) and percent of Cr(III) (e, right ordinate) after reaction at 540 min. Reaction conditions: $[ZVI]_0$ = 2.0 g/L, $[Cr(VI)]_{respike}$ = 2.0 mg/L, pH_{ini} = 5.0, [NaCl] = 1.0 mmol/L, t = 25 °C.

removal decreased slightly from 0.0083 to 0.0066 min^{-1} by ASZVI but sharply from 0.0031 to 0.0003 min^{-1} by SZVI. However, the corresponding reaction rate constants of ASZVI were 2.7–22.3 times higher than that of SZVI. Overall, there is a compatibility between sulfidation and partial aging, which can synergistically improve the reactive durability of ZVI, thus facilitating the application of ZVI-based technology for wastewater treatment.

3.3 Links of lgk_{SA} by ASZVI samples to their mass contents of iron and sulfur species

To interpret the coupled effects of sulfidation and partial aging on the reactivity of ZVI, the correlation of lgk_{SA} for the Cr(VI) removal by ASZVI samples with their contents of iron species at different depths was analyzed. First, it could be found that the mass contents of the Fe^{2+} in the subshell of ASZVI samples did not correlate with their lgk_{SA}. This result might be mainly due to the multiple Fe^{2+}-containing compounds (e.g., FeS_2 and FeS) formed in the subshells of ASZVI samples, making it difficult to find relevant trends from the perspective of the contents of the Fe^{2+}. However, the mass contents of Fe^{3+} on the surface of ASZVI samples showed a positive association with their lgk_{SA} (Fig. 4(a)). This relationship implies that the surficial Fe^{3+}-containing (hydr)oxides such as lepidocrocite and magnetite play a major role in sequestrating Cr(VI) since they can facilitate the mass transfer and electron transfer between the ASZVI and Cr(VI). In addition, the lgk_{SA} of ASZVI samples correlated well with their mass contents of Fe^0 in the subshell at 20 nm (Figs. 4(b)), which well echoed the fact that the target contaminant Cr(VI) could be highly reduced in the ASZVI redox system (Fig. 2(b)).

The next question is how ASZVI transfers the electrons from the Fe^0 core to the shell for the effective reduction of Cr(VI). Previous studies have shown that sulfidation can induce the formation of conductive FeS and FeS_2, which facilitates electron transfer from ZVI to contaminants (Zhao et al., 2005; Fan et al., 2017; Li et al., 2018; Gu et al., 2019; Ling et al., 2019; Xu et al., 2019a; 2019b; Li et al., 2020a; Cao et al., 2020a; Xu et al., 2020b). Generally, the reactivity of (nanoscale) SZVI materials are primarily influenced by the type and amount of reduced sulfurs (S^{2-} and S_2^{2-}) (Li et al., 2018; Xu et al., 2019b; Xu et al., 2020a; Cao et al., 2021a; Cao et al., 2021b; Xu et al., 2021). Meanwhile, researchers also found that the sulfidation methods and sulfur precursors could affect the distribution and speciation of sulfurs in (nanoscale) ZVI (Li et al., 2018; Cao et al., 2020b), ultimately affecting its reactivity. However, the available data do not yet have sufficient depth to specify the roles of the spatial sulfur species in mediating the reactivity of ZVI. As such, this section further explored the relationship between the contents of spatial sulfides in ASZVI samples and their rate constants for Cr(VI) removal.

As shown in Fig. 5, interestingly, the correlation coefficients (R) between the lgk_{SA} and the mass contents of S^{2-} and/or S_2^{2-} in the subshell of ASZVI samples at 5 nm were greater than 0.79, demonstrating that the subshells of S^{2-} and/or S_2^{2-} played a crucial role in

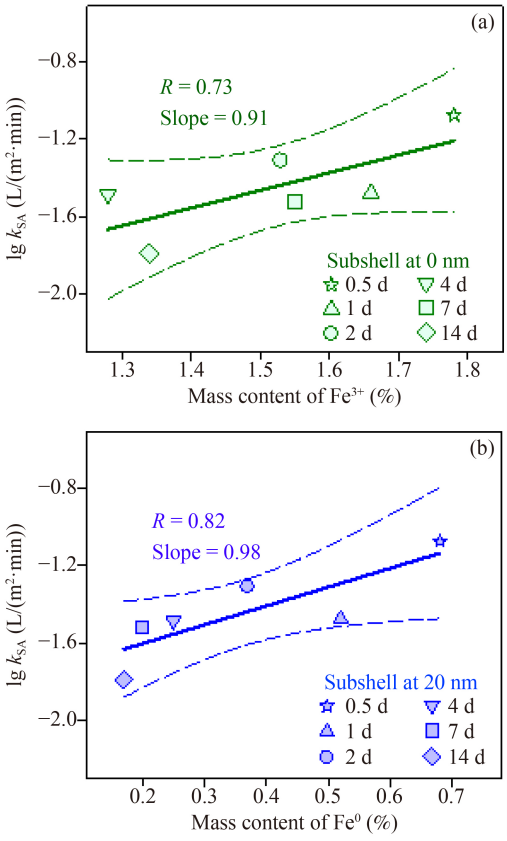

Fig. 4 Correlations of the specific rate constants (lg k_{SA}) for Cr(VI) removal by ASZVI samples with their mass contents of Fe^{3+} on the shell (a) and Fe^0 in the subshell at 20 nm (b).

mediating the reactivity of ASZVI samples. Since S^{2-} and S_2^{2-} can combine with Fe^{2+} to form the conductive FeS and FeS_2, we further suggest that the subshells of FeS and FeS_2 largely mediate the electron transfer of ASZVI from iron core to shell. In addition, it should be noted that the correlation coefficient and slope in the subshell of ASZVI at 5 nm were both higher than that at 20 nm. This significantly implies that the deeper the site of iron sulfides in the subshell of ASZVI, the weaker its contribution to the electron transfer of inner Fe^0 to outer. In other words, in the subshell at 20 nm, ASZVI could transfer efficiently electrons to the outer layer. Moreover, in terms of R^2 and slope, it is important to highlight that the correlations between the mass contents of S^{2-} in ASZVI samples and their reactivity toward Cr(VI) seemed to be stronger than that of S_2^{2-} (Figs. 5(a), 5(b), 5(d), and 5(e)). Since FeS is more conductive than FeS_2 (Kim et al., 2011), it can be inferred that the former can better modulate the reductive reactivity of ASZVI samples.

3.4 Mechanism of partial aging coupled with sulfidation to sustain the reactivity of ZVI

Based on the above correlation analysis, the reactivity of ASZVI should be highly dependent on its shell of the iron (hydr)oxides and subshell of the FeS_x. On the one hand, when the shell of ASZVI is magnetite, the conductive subshells of FeS and FeS_2 can couple with the conductive shell of magnetite to transfer the electrons of ASZVI for the reduction of Cr(VI). On the other hand, when the shell of ASZVI is lepidocrocite, it is also beneficial for the adsorption of Cr(VI), thus facilitating the transfer of the inner electron for Cr(VI) reduction. In addition, it should be addressed that a certain amount of FeS and FeS_2 in the outer subshells of ASZVI could also favor the encapsulation of the oxyanion Cr(VI) (Li et al., 2018), and thus benefiting the adsorption of Cr(VI) by ASZVI samples. Moreover, the FeS and FeS_2 on the surface of ASZVI could react with the Cr(VI) via the Eqs. (2)–(3) (Gong et al., 2017; Li et al., 2018; 2020a). Furthermore, these facts further corresponded well with the positive dependence of the lg k_{SA} of ASZVI samples on their mass contents of S^{2-} and/or S_2^{2-} in the subshell at 5 nm (Figs. 5(a)–5(c)).

$$3S^{2-} + 8HCrO_4^- + 32H^+ \rightarrow 3SO_4^{2-} + 8Cr^{3+} + 20H_2O \quad (2)$$

$$3S_2^{2-} + 15HCrO_4^- + 57H^+ \rightarrow 6SO_4^{2-} + 15Cr^{3+} + 36H_2O \quad (3)$$

In summary, our results suggested that: 1) the electron transfer of ASZVI from the Fe^0 core to the shell was largely mediated by the subshell of FeS and FeS_2. 2) Then, the shell of iron(hydr)oxides such as lepidocrocite and magnetite could also enable Cr(VI) mass transfer and ASZVI electron transfer, complementally favoring the Cr(VI) removal. 3) More importantly, the iron (hydr) oxides on the shell of ASZVI could in turn prevent the quenching of FeS and FeS_2 subshells by the natural substances (e.g., O_2, and H_2O/H^+), as illustrated in Figs. 1(e)–1(g) and S9. Therefore, the ASZVI was able to maintain excellent reactivity toward Cr(VI) under aerobic conditions. In general, the subshell of FeS and FeS_2 played a coupled role with the shell of iron (hydr)oxides in mediating the reactivity and durability of ASZVI toward Cr(VI), as concepted in Fig. 6.

4 Conclusions

The ability of SZVI-based system to maintain excellent reactivity with Cr(VI) over a long period of time is crucial for the successful treatment of wastewater. Previous researches have shown that sulfidation can improve the reactivity of ZVI by combining with FeS and FeS_2. However, it is unclear how to maintain the stability of the FeS and FeS_2 shells to sustain the reactivity of SZVI over time. In this study, we reconstructed the interface of SZVI by partial aging to obtain a highly reactive and durable structure consisting of Fe^0 core, FeS_x interlayer and iron (hydr)oxide shell. Correlation analysis showed that the specific rate constants of Cr(VI) removal by ASZVI samples were mainly related to their mass contents of S^{2-} and S_2^{2-} in the subshells, as well as their mass contents of Fe^{3+} on the surface and Fe^0 in the core.

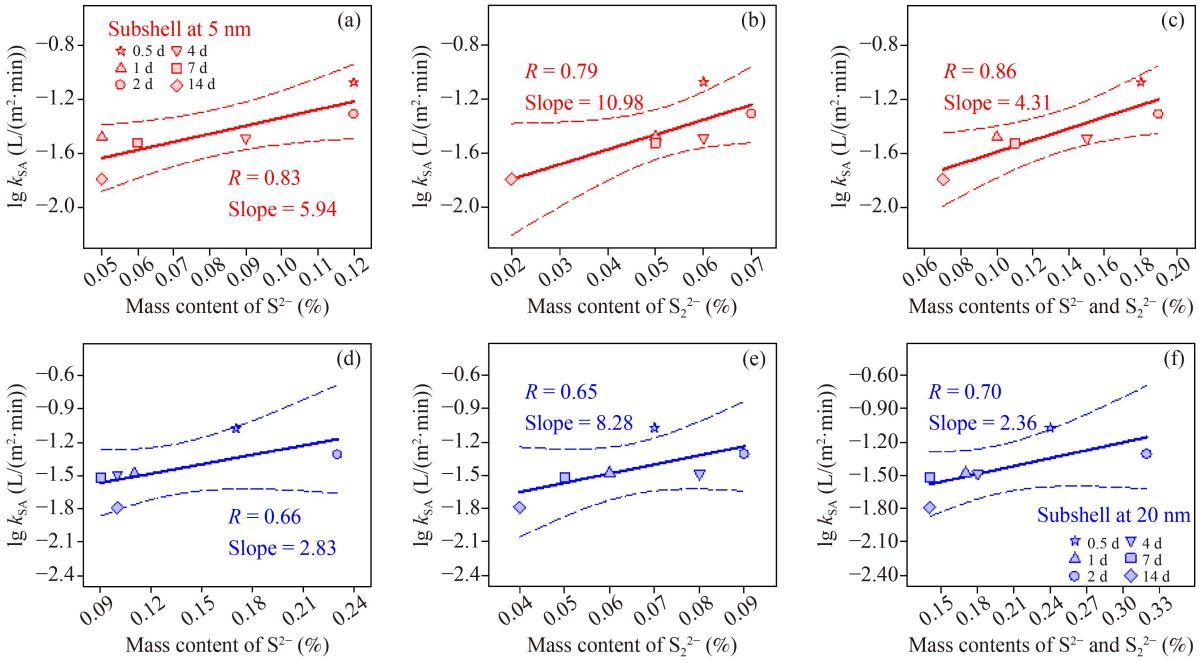

Fig. 5 Correlations of the specific rate constants (lg k_{SA}) for Cr(VI) removal by ASZVI samples with their mass contents of S^{2-} (a, d), S^{2-} (b, e), S^{2-} and S^{2-} (c, f) in the subshell at 5 nm (a–c) and 20 nm (d–f).

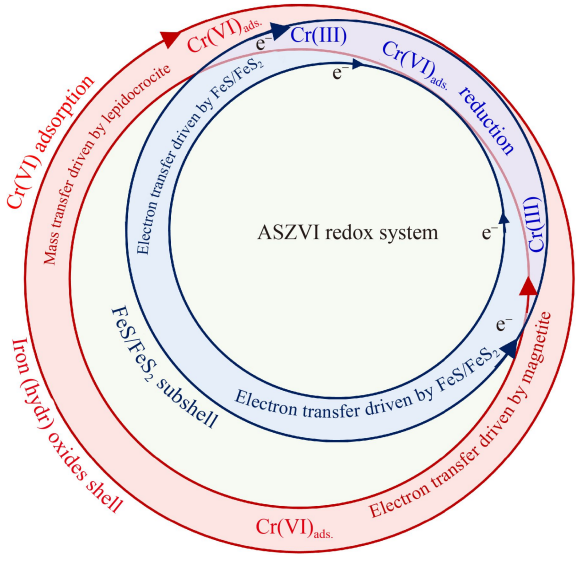

Fig. 6 Diagram of the reaction mechanism of Cr(VI) sequestration by ASZVI.

These results further suggested that the Fe^{3+}-containing lepidocrocite and magnetite on the shell of the ASZVI could couple with its conductive subshells of FeS and FeS_2 to facilitate the mass and electron transfer in ASZVI-Cr(VI) redox system. Moreover, the partial aging of SZVI allowed the stable embedding of FeS and FeS_2 into the subshell, resulting in efficient reduction of Cr(VI) by ASZVI. The structure-reactivity relationships identified in this study will contribute to a better understanding of how iron sulfides and iron (hydr)oxides modulate the reactive durability of SZVI. This finding will be valuable in the development of SZVI-based technology for wastewater treatment. Although the partial aging process is effective, it is also time-consuming and inconvenient. Therefore, there is a need to investigate alternative methods that are simpler and more efficient in reconstructing the interface of SZVI. It should be additionally noted that the aging period of SZVI in this study was relatively short compared to actual aging periods. Moreover, the wastewater being treated is a complex system that contains various ions and/or coexisting contaminants. Therefore, future studies should focus on evaluating the effectiveness of long-term aged SZVI for wastewater treatment under environmentally relevant conditions.

Acknowledgements This work was supported by the National Key R&D Program of China (No. 2021YFA1201701), the National Natural Science Foundation of China (No. 22025601), and the Postgraduate Research & Practice Innovation Program of Jiangsu Province (No. KYCX22_0495).

Conflict of Interest The authors declare that the research was conducted in the absence of any commercial or financial relationships that could be construed as a potential conflict of interest.

Electronic Supplementary Material Supplementary material is available in the online version of this article at https://doi.org/10.1007/s11783-024-1774-9 and is accessible for authorized users.

References

Agrawal A, Tratnyek P (1995). Reduction of nitro aromatic compounds by zero-valent iron metal. Environmental Science & Technology, 30(1): 153–160

Cai S, Chen B, Qiu X, Li J, Tratnyek P G, He F (2021). Sulfidation of zero-valent iron by direct reaction with elemental sulfur in water: efficiencies, mechanism, and dechlorination of trichloroethylene. Environmental Science & Technology, 55(1): 645–654

Cao Z, Li H, Lowry G V, Shi X, Pan X, Xu X, Henkelman G, Xu J (2021a). Unveiling the role of sulfur in rapid defluorination of florfenicol by sulfidized nanoscale zero-valent iron in water under ambient conditions. Environmental Science & Technology, 55(4): 2628–2638

Cao Z, Li H, Xu X, Xu J (2020a). Correlating surface chemistry and hydrophobicity of sulfidized nanoscale zerovalent iron with its reactivity and selectivity for denitration and dechlorination. Chemical Engineering Journal, 394: 124876

Cao Z, Li H, Zhang S, Hu Y, Xu J, Xu X (2021b). Properties and reactivity of sulfidized nanoscale zero-valent iron prepared with different borohydride amounts. Environmental Science. Nano, 8(9): 2607–2617

Cao Z, Xu J, Li H, Ma T, Lou L, Henkelman G, Xu X (2020b). Dechlorination and defluorination capability of sulfidized nanoscale zerovalent iron with suppressed water reactivity. Chemical Engineering Journal, 400: 125900

Fan D, Lan Y, Tratnyek P G, Johnson R L, Filip J, O'Carroll D M, Nunez Garcia A, Agrawal A (2017). Sulfidation of iron-based materials: a review of processes and implications for water treatment and remediation. Environmental Science & Technology, 51(22): 13070–13085

Fan P, Li L, Sun Y, Qiao J, Xu C, Guan X (2019a). Selenate removal by Fe^0 coupled with ferrous iron, hydrogen peroxide, sulfidation, and weak magnetic field: a comparative study. Water Research, 159: 375–384

Fan P, Sun Y, Zhou B, Guan X (2019b). Coupled effect of sulfidation and ferrous dosing on selenate removal by zerovalent iron under aerobic conditions. Environmental Science & Technology, 53(24): 14577–14585

Fan P, Zhang X, Deng H, Guan X (2021). Enhanced reduction of p-nitrophenol by zerovalent iron modified with carbon quantum dots. Applied Catalysis B: Environmental, 285: 119829

Feng P, Guan X, Sun Y, Choi W, Qin H, Wang J, Qiao J, Li L (2015). Weak magnetic field accelerates chromate removal by zero-valent iron. Journal of Environmental Sciences (China), 31: 175–183

Fu F, Dionysiou D D, Liu H (2014). The use of zero-valent iron for groundwater remediation and wastewater treatment: a review. Journal of Hazardous Materials, 267: 194–205

Garcia A N, Zhang Y, Ghoshal S, He F, O'Carroll D M (2021). Recent advances in sulfidated zerovalent iron for contaminant transformation. Environmental Science & Technology, 55(13): 8464–8483

Geiger C L, Ruiz N E, Clausen C A, Reinhart D R, Quinn J W (2002). Ultrasound pretreatment of elemental iron: kinetic studies of dehalogenation reaction enhancement and surface effects. Water Research, 36(5): 1342–1350

Gheju M (2011). Hexavalent chromium reduction with zero-valent iron (ZVI) in aquatic systems. Water, Air, and Soil Pollution, 222(1–4): 103–148

Gillham R W, Ohannesin S F (1994). Enhanced degradation of falogenated aliphatics by zero-valent iron. Ground Water, 32(6): 958–967

Gong Y, Gai L, Tang J, Fu J, Wang Q, Zeng E Y (2017). Reduction of Cr(VI) in simulated groundwater by FeS-coated iron magnetic nanoparticles. Science of the Total Environment, 595: 743–751

Gu Y, Gong L, Qi J, Cai S, Tu W, He F (2019). Sulfidation mitigates the passivation of zero valent iron at alkaline pHs: experimental evidences and mechanism. Water Research, 159: 233–241

Gu Y, Wang B, He F, Bradley M J, Tratnyek P G (2017). Mechanochemically sulfidated microscale zero valent iron: pathways, kinetics, mechanism, and efficiency of trichloroethylene dechlorination. Environmental Science & Technology, 51(21): 12653–12662

Guan X H, Sun Y K, Qin H J, Li J X, Lo I M, He D, Dong H R (2015). The limitations of applying zero-valent iron technology in contaminants sequestration and the corresponding countermeasures: the development in zero-valent iron technology in the last two decades (1994–2014). Water Research, 75: 224–248

Huang S, Xu C, Shao Q, Wang Y, Zhang B, Gao B, Zhou W, Tratnyek P G (2018). Sulfide-modified zerovalent iron for enhanced antimonite sequestration: characterization, performance, and reaction mechanisms. Chemical Engineering Journal, 338: 539–547

Huang X, Chen L, Ma Z, Carroll K C, Zhao X, Huo Z (2022). Cadmium removal mechanistic comparison of three Fe-based nanomaterials: water-chemistry and roles of Fe dissolution. Frontiers of Environmental Science & Engineering, 16(12): 151

Kim E J, Kim J H, Azad A M, Chang Y S (2011). Facile synthesis and characterization of Fe/FeS nanoparticles for environmental applications. ACS Applied Materials & Interfaces, 3(5): 1457–1462

Li H, Zhang J, Gu K, Li J (2020a). Sulfidation of zerovalent iron for improving the selectivity toward Cr(VI) in oxic water: involvements of FeS_x. Journal of Hazardous Materials, 409: 124498

Li J, Dou X, Qin H, Sun Y, Yin D, Guan X (2019). Characterization methods of zerovalent iron for water treatment and remediation. Water Research, 148: 70–85

Li J, Qin H, Guan X (2015). Premagnetization for enhancing the reactivity of multiple zerovalent iron samples toward various contaminants. Environmental Science & Technology, 49(24): 14401–14408

Li J, Zhang X, Liu M, Pan B C, Zhang W, Shi Z, Guan X (2018). Enhanced reactivity and electron selectivity of sulfidated zerovalent iron toward chromate under aerobic conditions. Environmental Science & Technology, 52(5): 2988–2997

Li J, Zhang X, Sun Y, Liang L, Pan B C, Zhang W, Guan X (2017).

Advances in sulfidation of zerovalent iron for water decontamination. Environmental Science & Technology, 248(23): 173–182

Li M, Mu Y, Shang H, Mao C, Cao S, Ai Z, Zhang L (2020b). Phosphate modification enables high efficiency and electron selectivity of nZVI toward Cr(VI) removal. Applied Catalysis B: Environmental, 263: 118364

Liang L, Sun W, Guan X, Huang Y, Choi W, Bao H, Li L, Jiang Z (2014a). Weak magnetic field significantly enhances selenite removal kinetics by zero valent iron. Water Research, 49: 371–380

Liang L P, Guan X H, Shi Z, Li J L, Wu Y N, Tratnyek P G (2014b). Coupled effects of aging and weak magnetic fields on sequestration of selenite by zero-valent iron. Environmental Science & Technology, 48(11): 6326–6334

Ling J, Qiao J, Song Y, Sun Y (2019). Influence of coexisting ions on the electron efficiency of sulfidated zerovalent iron toward Se(VI) removal. Chemical Engineering Journal, 378: 122124

Liou Y H, Lo S L, Lin C J, Kuan W H, Weng S C (2005). Effects of iron surface pretreatment on kinetics of aqueous nitrate reduction. Journal of Hazardous Materials, 126(1): 189–194

Liu Y, Qiao J, Sun Y, Guan X (2022). Simultaneous sequestration of humic acid-complexed Pb(II), Zn(II), Cd(II), and As(V) by sulfidated zero-valent iron: performance and stability of sequestration products. Environmental Science & Technology, 56(5): 3127–3137

Lü Y, Li J, Li Y, Liang L, Dong H, Chen K, Yao C, Li Z, Li J, Guan X (2019). The roles of pyrite for enhancing reductive removal of nitrobenzene by zero-valent iron. Applied Catalysis B: Environmental, 242: 9–18

Mangayayam M, Dideriksen K, Ceccato M, Tobler D J (2019). The structure of sulfidized zero-valent iron by one-pot synthesis: impact on contaminant selectivity and long-term performance. Environmental Science & Technology, 53(8): 4389–4396

Matheson L J, Tratnyek P G (1994). Reductive dehalogenation of chlorinated methanes by iron metal. Environmental Science & Technology, 28(12): 2045–2053

Miehr R, Tratnyek P G, Bandstra J Z, Scherer M M, Alowitz M J, Bylaska E J (2004). Diversity of contaminant reduction reactions by zerovalent iron: Role of the reductate. Environmental Science & Technology, 38(1): 139–147

Noubactep C (2008). A critical review on the process of contaminant removal in Fe^0-H_2O systems. Environmental Technology, 29(8): 909–920

Qiao J, Liu Y, Yang H, Guan X, Sun Y (2021). Remediation of arsenic contaminated soil by sulfidated zero-valent iron. Frontiers of Environmental Science & Engineering, 15(5): 83

Qin H, Guan X, Bandstra J Z, Johnson R L, Tratnyek P G (2018). Modeling the kinetics of hydrogen formation by zerovalent iron: effects of sulfidation on micro- and nano-scale particles. Environmental Science & Technology, 52(23): 13887–13896

Qin H J, Li J X, Yang H Y, Pan B C, Zhang W M, Guan X H (2017). Coupled effect of ferrous ion and oxygen on the electron selectivity of zerovalent iron for selenate sequestration. Environmental Science & Technology, 51(9): 5090–5097

Rajajayavel S R, Ghoshal S (2015). Enhanced reductive dechlorination of trichloroethylene by sulfidated nanoscale zerovalent iron. Water Research, 78: 144–153

Shao Q, Xu C, Wang Y, Huang S, Zhang B, Huang L, Fan D, Tratnyek P G (2018). Dynamic interactions between sulfidated zerovalent iron and dissolved oxygen: mechanistic insights for enhanced chromate removal. Water Research, 135: 322–330

Shi J, Zhang J, Wang C, Liu Y, Li J (2023). Research progress on the magnetite nanoparticles in the fields of water pollution control and detection. Chemosphere, 336: 139220

Song S, Su Y, Adeleye A S, Zhang Y, Zhou X (2017). Optimal design and characterization of sulfide-modified nanoscale zerovalent iron for diclofenac removal. Applied Catalysis B: Environmental, 201: 211–220

Stookey L L (1970). Ferrozine—a new spectrophotometric reagent for iron. Analytical Chemistry, 42(7): 779–781

Sun Y K, Guan X H, Wang J M, Meng X G, Xu C H, Zhou G M (2014). Effect of weak magnetic field on arsenate and arsenite removal from water by zerovalent iron: an XAFS investigation. Environmental Science & Technology, 48(12): 6850–6858

Ullah S, Guo X, Luo X, Zhang X, Li Y, Zhang Z (2020). The coupling of sand with ZVI/oxidants achieved proportional and highly efficient removal of arsenic. Frontiers of Environmental Science & Engineering, 14(6): 94

Xu C, Zhang B, Wang Y, Shao Q, Zhou W, Fan D, Bandstra J Z, Shi Z, Tratnyek P G (2016a). Effects of sulfidation, magnetization, and oxygenation on azo dye reduction by zerovalent iron. Environmental Science & Technology, 50(21): 11879–11887

Xu H, Sun Y, Li J, Li F, Guan X (2016b). Aging of zerovalent iron in synthetic groundwater: X-ray photoelectron spectroscopy depth profiling characterization and depassivation with uniform magnetic field. Environmental Science & Technology, 50(15): 8214–8222

Xu J, Avellan A, Li H, Clark E A, Henkelman G, Kaegi R, Lowry G V (2020a). Iron and sulfur precursors affect crystalline structure, speciation, and reactivity of sulfidized nanoscale zerovalent iron. Environmental Science & Technology, 54(20): 13294–13303

Xu J, Avellan A, Li H, Liu X, Noël V, Lou Z, Wang Y, Kaegi R, Henkelman G, Lowry G V (2020b). Sulfur loading and speciation control the hydrophobicity, electron transfer, reactivity, and selectivity of sulfidized nanoscale zerovalent iron. Advanced Materials, 32(17): 1906910

Xu J, Cao Z, Zhou H, Lou Z, Wang Y, Xu X, Lowry G V (2019a). Sulfur dose and sulfidation time affect reactivity and selectivity of post-sulfidized nanoscale zerovalent iron. Environmental Science & Technology, 53(22): 13344–13352

Xu J, Li H, Lowry G V (2021). Sulfidized nanoscale zero-valent iron: tuning the properties of this complex material for efficient groundwater remediation. Accounts of Materials Research, 2(6): 420–431

Xu J, Wang Y, Weng C, Bai W, Jiao Y, Kaegi R, Lowry G V (2019b). Reactivity, selectivity, and long-term performance of sulfidized nanoscale zerovalent iron with different properties. Environmental Science & Technology, 53(10): 5936–5945

Xu W, Li Z, Shi S, Qi J, Cai S, Yu Y, O'Carroll D M, He F (2020c). Carboxymethyl cellulose stabilized and sulfidated nanoscale zero-valent iron: characterization and trichloroethene dechlorination. Applied Catalysis B: Environmental, 262: 118303

Yao W, Zhang J, Gu K, Li J, Qian J (2022). Synthesis, characterization

and performances of green rusts for water decontamination: a review. Environmental Pollution, 304: 119205

Yoon I H, Kim K W, Bang S, Kim M G (2011). Reduction and adsorption mechanisms of selenate by zero-valent iron and related iron corrosion. Applied Catalysis B: Environmental, 104(1): 185–192

Zhang X, Li J, Sun Y, Li L, Pan B, Zhang W, Guan X (2018). Aging of zerovalent iron in various coexisting solutes: characteristics, reactivity toward selenite and rejuvenation by weak magnetic field. Separation and Purification Technology, 191: 94–100

Zhao J, Su A, Tian P, Tang X, Collins R N, He F (2021). Arsenic (III) removal by mechanochemically sulfidated microscale zero valent iron under anoxic and oxic conditions. Water Research, 198: 117132

Zhao J M, Wei Z, Zuo Y, Zhao X H (2005). Effects of some ions on ion-selectivity of ferrous sulfide film. Journal of Applied Electrochemistry, 35(3): 267–271

Zou H, Hu E, Yang S, Gong L, He F (2019). Chromium(VI) removal by mechanochemically sulfidated zero valent iron and its effect on dechlorination of trichloroethene as a co-contaminant. Science of the Total Environment, 650: 419–426